# Dynamic critical behavior of an extended reptation dynamics for self-avoiding walks

Sergio Caracciolo,[1,*] Mauro Papinutto,[2,†] and Andrea Pelissetto[3,‡]
[1]*Dipartmento di Fisica dell'Università di Milano, I-20133 Milano, Sez. INFN di Pisa, and NEST-INFM, I-56100 Pisa, Italy*
[2]*Dipartmento di Fisica dell'Università di Pisa and Sez. INFN di Pisa, I-56100 Pisa, Italy*
[3]*Dipartmento di Fisica dell'Università di Roma "La Sapienza" and Sez. INFN di Roma I, I-00185 Roma, Italy*
(Received 22 October 2001; published 28 February 2002)

We consider lattice self-avoiding walks and discuss the dynamic critical behavior of two dynamics that use local and bilocal moves and generalize the usual reptation dynamics. We determine the integrated and exponential autocorrelation times for several observables, perform a dynamic finite-size scaling study of the autocorrelation functions, and compute the associated dynamic critical exponents $z$. For the variables that describe the size of the walks, in the absence of interactions we find $z \approx 2.2$ in two dimensions and $z \approx 2.1$ in three dimensions. At the $\theta$ point in two dimensions we have $z \approx 2.3$.

DOI: 10.1103/PhysRevE.65.031106 PACS number(s): 05.40.−a, 05.10.Ln, 36.20.−r, 61.25.Hq

## I. INTRODUCTION

The lattice self-avoiding walk (SAW) is a well-known model for the critical behavior of a homopolymer in a solvent [1,2] and it has also been extensively used in the study of several properties of heteropolymers [3,4]. The earliest simulations either used a local dynamics [5] in which, at each step, a small part of the walk (usually 2–4 consecutive beads) was modified, or the so-called reptation dynamics [6–9]. All these algorithms are, however, nonergodic [7,8,10–12] and only a limited fraction of the phase space is visited. Note that, contrary to some claims in the literature, the deviations are sizable even for very short walks if one is interested in low-temperature properties, i.e., polymers in the compact phase or heteropolymers near the folding temperature [13–15]. For instance—see footnote 4 in Ref. [16]—if one uses the Verdier-Stockmayer algorithm [5] in two dimensions, one does not sample 3.2%, 1.4%, 5% of the most compact configurations for $N=11,13,15$. These ergodicity problems can be solved by using a different ensemble [17–20], chain-growth algorithms [21–24], or nonlocal algorithms [25–30]. However, in the presence of interactions, nonlocal algorithms become inefficient since nonlocal moves generate new walks with large energy differences and thus they will be rejected making the dynamics very slow. Chain-growth algorithms may work much better but, in order to make them efficient, one must sample a different probability distribution, and thus one may be worried by the introduced bias.

In this paper, we wish to discuss a family of dynamics that use bilocal moves and generalize the reptation dynamics: a bilocal move alters at the same time two disjoint small groups of consecutive sites of the walk that may be very far away. Since a small number of beads is changed at each step, these algorithms should be efficient in the presence of interactions, and thus they can be used in the study of the collapsed phase and of the folding of heteropolymers. Similar moves were introduced in Refs. [31–34].

The ergodicity properties of these algorithms have been discussed in Ref. [16]. Here, we will study the dynamic properties of two different implementations. The first one, the extended end-end reptation (EER) algorithm, is obtained by performing at the same time reptation moves and bilocal kink-kink moves. Such an algorithm is quite efficient. In the absence of interactions, the autocorrelation time for quantities that measure the size of the walk—for instance, the end-to-end distance or the radius of gyration—scales as $N^z$ with $z \approx 2.2$ in two dimensions and $z \approx 2.1$ in three dimensions. The behavior of the energy (number of nearest-neighbor contacts among nonconsecutive links) is even faster, with $z \approx 1.7$ in both dimensions. We have also tested the behavior of the algorithm at the $\theta$ point in two dimensions. We find that the critical behavior is only marginally worse, with $z \approx 2.3$, both for metric quantities and for the energy. We have also studied a different version, the extended kink-end reptation (KER) algorithm, in which the reptation moves are replaced by kink-end moves, i.e., by moves in which a kink is cleaved and two additional links are attached at the end of the walk and vice versa. This version is much slower, with $z \approx 2.9$ for quantities that measure the polymer size. Clearly, reptation moves are essential to obtain a fast dynamics.

The paper is organized as follows. In Sec. II, we define the model and the observables whose critical behavior will be studied. In Sec. III, we define the basic moves and the two dynamics. Specific implementation details are reported in the Appendix. In Sec. IV, we define the autocorrelation times, the dynamic critical exponents, and the methods we use to compute them. In Sec. V and Sec. VI, we discuss the critical behavior of the EER and of the KER algorithms in the absence of interactions, while in Sec. VII we discuss the behavior of the EER algorithm in two dimensions at the $\theta$ point. Conclusions are presented in Sec. VIII.

## II. DEFINITIONS

In this paper, we consider SAWs with a fixed number of steps $N$ and free end points on a hypercubic lattice $\mathbb{Z}^d$. An

*Email address: Sergio.Caracciolo@sns.it
†Email address: papinutt@cibs.sns.it
‡Email address: Andrea.Pelissetto@roma1.infn.it

 

$N$-step SAW $\omega$ is a set of $N+1$ lattice sites $\omega_0, \ldots, \omega_N$, such that $\omega_i$ and $\omega_{i+1}$ are lattice nearest neighbors, and $\omega_i \neq \omega_j$. By translation invariance we may fix $\omega_0$ to be the origin.

We consider several observables that measure the size of an $N$ step SAW:

The mean square end-to-end distance

$$R_e^2 \equiv (\omega_N - \omega_0)^2. \tag{1}$$

The mean square radius of gyration

$$R_g^2 \equiv \frac{1}{N+1} \sum_{i=0}^{N} \left( \omega_i - \frac{1}{N+1} \sum_{k=0}^{N} \omega_k \right)^2 = \frac{1}{2(N+1)^2} \sum_{i,j=0}^{N} (\omega_i - \omega_j)^2. \tag{2}$$

The mean square monomer distance from an end point

$$R_m^2 \equiv \frac{1}{N+1} \sum_{i=0}^{N} (\omega_i - \omega_0)^2. \tag{3}$$

Moreover, for each SAW, we define the number of nearest-neighbor contacts $\mathcal{E}$. It is defined as follows. For every $i \neq j$ we define

$$c_{ij} \equiv \begin{cases} 1 & \text{if } |\omega_i - \omega_j| = 1, \\ 0 & \text{otherwise.} \end{cases} \tag{4}$$

Then,

$$\mathcal{E} \equiv - \sum_{i=0}^{N-2} \sum_{j=i+2}^{N} c_{ij}. \tag{5}$$

Note that we do not include here the trivial contacts between consecutive walk sites.

We give each SAW $\omega$ a weight $W(\beta)$ depending on the inverse temperature $\beta \equiv 1/kT$,

$$W(\beta) \equiv \frac{1}{Z_N} e^{-\beta \mathcal{E}}, \tag{6}$$

where $Z_N$ is the partition sum. The mean values $\langle R_e^2 \rangle_N$, $\langle R_g^2 \rangle_N$, and $\langle R_m^2 \rangle_N$ have the asymptotic behavior $N^{2\nu}$ as $N \to \infty$, where $\nu$ is a critical exponent, which is independent of the microscopic details of the lattice model but depends on $\beta$. For $\beta < \beta_\theta$ (good-solvent regime) the SAW is swollen: $\nu = 3/4$ in two dimensions and [35] $\nu = 0.58758(7)$ in three dimensions (see Ref. [36] for a review of estimates of $\nu$ in three dimensions). For $\beta > \beta_\theta$ the SAW is compact with $\nu = 1/d$. For the very specific value $\beta = \beta_\theta$ ($\theta$ point),

$$\nu = \begin{cases} \dfrac{4}{7}, & d=2 \quad (\text{Ref. } [37]), \\ \dfrac{1}{2} \times \ln, & d=3 \quad (\text{Refs. } [1,38-41]). \end{cases} \tag{7}$$

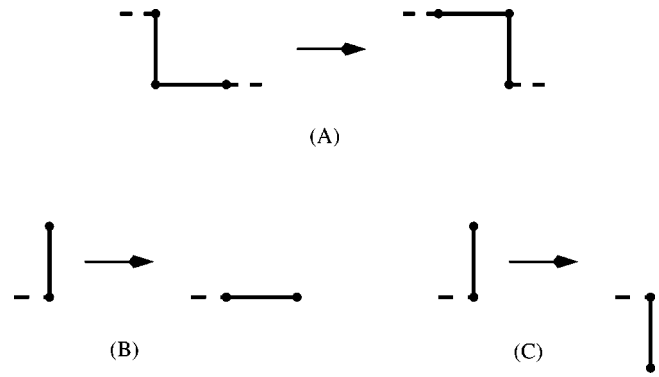


FIG. 1. All one-bead moves: (a) One-bead flip. (b) 90° end-bond rotation. (c) 180° end-bond rotation.

The critical value $\beta_\theta$ depends on the model, on the lattice type, and on all microscopic details. For the model we consider here we have: on the square lattice $\beta_\theta = 0.665(2)$ (Ref. [42]) and $\beta_\theta = 0.667(1)$ (Ref. [43]); on the cubic lattice $\beta_\theta = 0.276(6)$ (Ref. [44]) and $\beta_\theta = 0.2690(2)$ (Ref. [23]).

## III. ALGORITHMS

For the simulation of weakly interacting walks, i.e., for $\beta < \beta_\theta$, there exist powerful nonlocal algorithms [27,30]. However, these algorithms cannot be used in confined geometries—they are not ergodic—and are very inefficient in the presence of strong interactions. Indeed, in these conditions nonlocal moves are rarely accepted. In this paper, we consider two algorithms that use local and bilocal moves [16]. A local move is the one that alters only a few consecutive beads of the SAW, leaving the other sites unchanged. A bilocal move is instead the one that alters two disjoint small groups of consecutive sites of the walk; these two groups may, in general, be very far from each other.

In our study we consider two types of local moves (see Fig. 1):

(L0) One-bead flips in which one *internal* bead [i.e., $\omega(i)$, $1 \leq i \leq N-1$] only is moved.

(L1) End-bond rotations in which the last step of the walk is rotated.

We also introduce several types of bilocal moves:

(B22) Kink-transport moves in which a kink is cleaved from the walk and attached at a pair of neighboring sites somewhere else along the walk (see Fig. 2); note that the

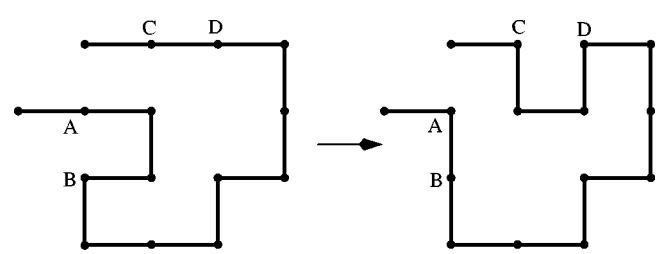


FIG. 2. The kink-transport move. A kink has been cleaved from AB and attached at CD. Note that the new kink is permitted to occupy one or both of the sites abandoned by the old kink.

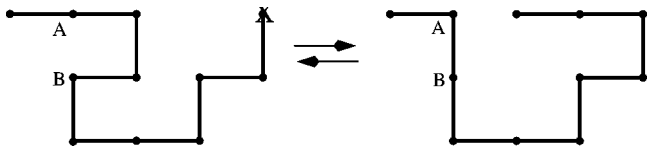


FIG. 3. The kink-end reptation (→) and end-kink reptation (←) moves. In (→), a kink has been cleaved from AB and two new steps have been attached at the end marked X. Note that the new end steps are permitted to occupy one or both of the sites abandoned by the kink.

new kink is allowed to occupy one or both of the sites abandoned by the old kink.

(BKE) Kink-end and end-kink reptation moves (see Fig. 3). In the kink-end reptation move a kink is deleted at one location along the walk and two new bonds are appended in arbitrary directions at the free end point of the walk. On the contrary, an end-kink reptation move is characterized by deletion of two bonds from the end of the walk and insertion of a kink, in arbitrary orientation, at some location along the walk.

(BEE) Reptation move in which one bond is deleted from one end of the walk and a new bond is appended in arbitrary direction at the other end.

Using these elementary moves we introduce three different updates that leave invariant the Gibbs measure (6). They are described in detail in the Appendix. We will then consider two algorithms: (a) extended end-end reptation (EER) algorithm; (b) extended kink-end reptation (KER) algorithm.

The EER algorithm consists in combining with nonzero probability the reptation move and the kink-kink local/bilocal move, see Sec. 1 and Sec. 2 of the Appendix for the implementation details. More precisely, with probability $p$ one performs a reptation move, and with probability $1-p$ a kink-kink local/bilocal move. The KER algorithm works analogously: instead of the reptation moves, we use the kink-end/end-kink BKE moves. Both algorithms are known to be ergodic in two dimensions, while for $d=3$ ergodicity has been proved only for the KER algorithm [16]. For the EER algorithm ergodicity is still an open problem. The probability $p$ is not fixed, and can be tuned to obtain the fastest dynamics. However, it should not have any influence on the dynamic critical behavior, i.e., on the dynamic critical exponents. For this reason we have not performed a systematic study of the dependence of the numerical results on $p$ and we have simply set $p=0.50$ in most of our simulations.

In order to have a fast and efficient implementation, it is important that local and bilocal moves are performed in a CPU time of order one, i.e., constant as $N\to\infty$. This can be obtained only with a careful choice of the data structures used to store the walk coordinates. For local and end-end reptation moves it is sufficient to store the walk coordinates as a circular list in which the coordinates of the beads are stored sequentially. However, such a data structure is not convenient for B22 and BKE moves, since in this case insertion and deletion of a single point requires a time of order $N$. The problem is solved [45] by storing the coordinates in a *contiguously allocated doubly linked linear list*. The coordinates are stored contiguously but not in any particular order. In order to find the bead that follows and precedes a given one, one keeps two arrays of pointers that give the location in the coordinate list of the preceding and of the successive walk bead. With this type of data structure, insertions and deletions take a time of order one. An efficient implementation requires also the ability to perform the self-avoidance check in a time of order one. This may be obtained by using a bit table—however, this is only possible for short walks—or a hash table. In this second case, one must be careful to use a hashing method that allows to insert and delete a single point in a time of order one. A very efficient method is described in Ref. [46].

## IV. DYNAMIC BEHAVIOR

In order to determine the efficiency of the dynamics, we study the critical behavior of the autocorrelation times. Quite generally, given an observable $A$, we define the unnormalized autocorrelation function

$$C_{AA}(t)\equiv\langle A_s A_{s+t}\rangle-\langle A\rangle^2, \tag{8}$$

and its normalized counterpart,

$$\rho_{AA}\equiv C_{AA}(t)/C_{AA}(0), \tag{9}$$

where $t$ is the dynamics "time." Typically, $\rho_{AA}(t)$ decays exponentially, i.e., $\rho_{AA}(t)\sim e^{-|t|/\tau}$, for large $|t|$. We define the *exponential* autocorrelation time

$$\tau_{\exp,A}=\limsup_{|t|\to+\infty}\frac{|t|}{-\ln|\rho_{AA}(t)|}, \tag{10}$$

and the *integrated* autocorrelation time

TABLE I. Exponential autocorrelation times for the EER algorithm in two and three dimensions. "iter." is the number of iterations.

| $d$ | $N$ | iter. | $\tau_{\exp,R_g^2}$ | $\tau_{\exp,R_e^2}$ | $\tau_{\exp,R_m^2}$ | $\tau_{\exp,\mathcal{E}}$ |
|---|---|---|---|---|---|---|
| | 100 | $5.77\times10^{10}$ | $3230\pm20$ | $3062\pm24$ | $3190\pm16$ | $3078\pm40$ |
| 2 | 300 | $5.38\times10^{11}$ | $43600\pm900$ | $47300\pm1500$ | $43140\pm760$ | $35600\pm1260$ |
| | 1000 | $6.90\times10^{11}$ | $710400\pm42000$ | $859600\pm46000$ | $745000\pm36000$ | $448000\pm30000$ |
| | 100 | $4.36\times10^{10}$ | $2980\pm40$ | $3020\pm30$ | $2968\pm30$ | $2840\pm60$ |
| 3 | 300 | $4.42\times10^{11}$ | $32640\pm840$ | $34700\pm900$ | $32980\pm840$ | $27480\pm800$ |
| | 1000 | $5.20\times10^{11}$ | $370400\pm22000$ | $374800\pm24000$ | $368000\pm22000$ | $300800\pm16000$ |

$$\tau_{\mathrm{int},A}=\frac{1}{2}\sum_{s=-\infty}^{+\infty}\rho_{AA}(s)=\frac{1}{2}+\sum_{s=1}^{+\infty}\rho_{AA}(s). \tag{11}$$

The factor 1/2 is inserted so that $\tau_{\mathrm{int},A}\approx\tau_{\mathrm{exp},A}$ if $\rho_{AA}(t)=e^{-|t|/\tau_{\mathrm{exp},A}}$ with $\tau_{\mathrm{exp},A}\gg 1$.

In order to estimate $\tau_{\mathrm{exp},A}$, we will proceed as follows. If $\hat{\rho}_{AA}(t)$ is the normalized autocorrelation function estimated from the data, we define an effective exponent

$$\hat{\tau}_{\mathrm{exp},A}(t;s)\equiv s\left[\ln\left(\frac{\hat{\rho}_{AA}(t)}{\hat{\rho}_{AA}(t+s)}\right)\right]^{-1}, \tag{12}$$

where $s$ is some fixed number. This quantity should become independent of $t$ as $t\to\infty$. In practice, we look for a region in which the estimates are sufficiently stable with $t$ and then take the value of $\hat{\tau}_{\mathrm{exp},A}(t;s)$ in this region as our estimate of $\tau_{\mathrm{exp},A}$. In order to apply the method we should also choose the parameter $s$. It should be neither too small, i.e., $s\ll\tau_{\mathrm{exp},A}$, otherwise $\hat{\rho}_{AA}(t)\approx\hat{\rho}_{AA}(t+s)$, nor too large, i.e., $s\gg\tau_{\mathrm{exp},A}$, otherwise the error on $\hat{\rho}_{AA}(t+s)$ is large. In our study, we have always fixed $s$ self-consistently, by taking $s\approx\tau_{\mathrm{exp},A}/k$ with $k\approx 10$–20.

In order to estimate $\tau_{\mathrm{int},A}$, we use the self-consistent windowing method proposed in Ref. [10]. We define our estimate as

$$\hat{\tau}_{\mathrm{int},A}=\frac{1}{2}\sum_{t=-M}^{M}\hat{\rho}_{AA}(t), \tag{13}$$

where $M$ is the smallest integer that satisfies $M\geq c\,\hat{\tau}_{\mathrm{int},A}$ and $c$ is a fixed constant. The variance of $\hat{\tau}_{\mathrm{int},A}$ is given by

$$\mathrm{var}(\hat{\tau}_{\mathrm{int},A})\approx\frac{2(2M+1)}{n}\hat{\tau}^2_{\mathrm{int},A}, \tag{14}$$

where $n$ is the number of Monte Carlo iterations and we have made the approximation $\tau_{\mathrm{int},A}\ll M\ll n$. The method provides quite accurate estimates of $\hat{\tau}_{\mathrm{int},A}$ as long as $c$ is chosen so that $M$ is a few times $\tau_{\mathrm{exp},A}$. There are cases in which $\tau_{\mathrm{int},A}\ll\tau_{\mathrm{exp},A}$, so that the previous condition is difficult to satisfy. In this case, a successful *ad hoc* recipe was proposed by Li *et al.* [47] for the pivot algorithm. They noted that, when $A$ is one of the radii, $\rho_{AA}(t)\approx 1/t^q$ in the intermediate region $\tau_{\mathrm{int},A}\ll t\lesssim\tau_{\mathrm{exp},A}$, with $q\approx 1$–1.2. Thus, they extrapolated $\rho_{AA}(t)$ proportionally to $1/t$ for $t>M$, [i.e., set $\hat{\rho}_{AA}(t)=M\hat{\rho}_{AA}(M)/t$ for $t>M$], and then used this expression to compute the contribution to $\tau_{\mathrm{int},A}$ from the region $M<t<\tau_{\mathrm{exp},A}$. This gives the modified estimate

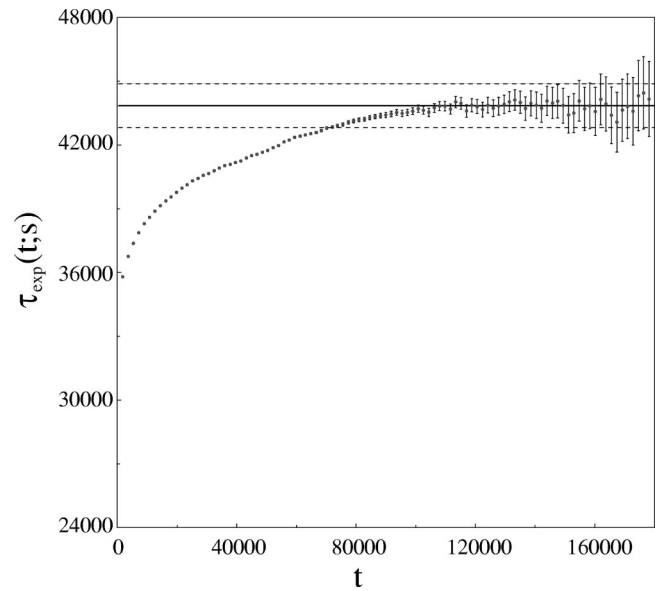


FIG. 4. Effective exponent $\hat{\tau}_{\mathrm{exp},R_g^2}(t;s)$ for the EER algorithm. Here $d=2$, $N=300$, $s=2000$. The horizontal line corresponds to our final estimate $\tau_{\mathrm{exp},R_g^2}=43\,600$ and the dashed lines to $\pm$ one error bar (900).

$$\tilde{\tau}_{\mathrm{int},A}=\frac{1}{2}\sum_{t=-M}^{+M}\hat{\rho}_{AA}(t)+M\hat{\rho}_{AA}(M)\ln\left(\frac{\tau_{\mathrm{exp},A}}{M}\right). \tag{15}$$

In general, the autocorrelation times diverge as $N\to\infty$. We can thus define two dynamic critical exponents $z_{\mathrm{exp},A}$ and $z_{\mathrm{int},A}$ by

$$\tau_{\mathrm{int},A}\sim N^{z_{\mathrm{int},A}},$$
$$\tau_{\mathrm{exp},A}\sim N^{z_{\mathrm{exp},A}}. \tag{16}$$

The dynamic critical exponents can also be obtained by requiring the autocorrelation function to obey a dynamic scaling law of the form [45,48,49]

$$\rho_{AA}(t;N)\approx|t|^{-a}F_{AA}(tN^{-b})\approx N^{-ab}G_{AA}(tN^{-b}), \tag{17}$$

TABLE II. Dynamic exponent $z_{\mathrm{exp}}$ for the EER algorithm in two and three dimensions, obtained by fitting $\tau_{\mathrm{exp}}=BN^{z_{\mathrm{exp}}}$. The number of degrees of freedom of the fit is 1.

| $d$ | | $\tau_{\mathrm{exp},R_g^2}$ | $\tau_{\mathrm{exp},R_e^2}$ | $\tau_{\mathrm{exp},R_m^2}$ | $\tau_{\mathrm{exp},\mathcal{E}}$ |
|---|---|---|---|---|---|
| | $z_{\mathrm{exp}}$ | $2.37\pm0.02$ | $2.46\pm0.02$ | $2.36\pm0.02$ | $2.18\pm0.02$ |
| 2 | $B$ | $0.0610\pm0.0048$ | $0.0376\pm0.0032$ | $0.0586\pm0.0030$ | $0.133\pm0.013$ |
| | $\chi^2$ | 1.18 | 1.03 | 0.52 | 2.33 |
| | $z_{\mathrm{exp}}$ | $2.10\pm0.03$ | $2.11\pm0.04$ | $2.10\pm0.03$ | $2.04\pm0.03$ |
| 3 | $B$ | $0.196\pm0.032$ | $0.180\pm0.028$ | $0.190\pm0.030$ | $0.242\pm0.028$ |
| | $\chi^2$ | 1.13 | 1.90 | 1.31 | 1.57 |

TABLE III. Integrated autocorrelation times for the EER algorithm in two and three dimensions.

| $d$ | $N$ | $\tau_{\mathrm{int},R_g^2}$ | $\tau_{\mathrm{int},R_e^2}$ | $\tau_{\mathrm{int},R_m^2}$ | $\tau_{\mathrm{int},\mathcal{E}}$ |
|---|---|---|---|---|---|
| | 100 | $3113.6\pm5.6$ | $2209.2\pm3.4$ | $2124.4\pm3.2$ | $861.64\pm0.82$ |
| 2 | 300 | $36000\pm72$ | $24250\pm40$ | $23764\pm38$ | $5596.4\pm4.4$ |
| | 1000 | $522880\pm3520$ | $337220\pm1820$ | $334600\pm1800$ | $39224\pm72$ |
| | 100 | $2729.0\pm5.2$ | $1761.2\pm2.8$ | $1780.0\pm2.8$ | $925.4\pm1.0$ |
| 3 | 300 | $27092\pm52$ | $16772\pm26$ | $17162\pm26$ | $6035.8\pm5.4$ |
| | 1000 | $332900\pm2100$ | $199160\pm960$ | $205100\pm1000$ | $42954\pm96$ |

valid in the limit $N\to\infty$, $|t|\to\infty$, with $tN^{-b}$ fixed. Here, $a,b>0$ are dynamic critical exponents and $F_{AA}$ and $G_{AA}$ are suitable scaling functions. If $F_{AA}(x)$ is continuous, strictly positive, and rapidly decaying—e.g., exponentially—as $|x|\to\infty$, then, it is not hard to see that

$$z_{\mathrm{exp},A}=b, \tag{18}$$

$$z_{\mathrm{int},A}=(1-a)b \quad (\text{if } a<1). \tag{19}$$

The exponents $a$ and $b$ can be determined by requiring the collapse onto a single curve of the autocorrelation functions corresponding to different values of $N$. Then, using the previous formulas, one can determine $z_{\mathrm{exp},A}$ and $z_{\mathrm{int},A}$. The advantage of this method is in its bypassing the problem of determining $\tau_{\mathrm{exp},A}$ and $\tau_{\mathrm{int},A}$, but it is quite difficult to assess the errors, since the optimal values are determined visually.

## V. THE EER DYNAMICS IN TWO AND THREE DIMENSIONS

We performed an extensive Monte Carlo simulation of noninteracting ($\beta=0$) SAWs on the square lattice, $d=2$, and on the cubic lattice, $d=3$, using the EER algorithm. We set $p=0.5$ and used the first version of the reptation move, see Sec. B of the Appendix. We considered only three values of $N$, $N=100,300,1000$, but for each of them we collected a very large statistics, see Table I. We measured $\langle R_g^2\rangle_N$, $\langle R_e^2\rangle_N$, $\langle R_m^2\rangle_N$, and the energy $\mathcal{E}_N$, i.e., the number of nearest-neighbor contacts. We compared the static results of our simulations with those of Li *et al.* [47], finding good agreement.

First of all, we measured the exponential autocorrelation times. As an example, in Fig. 4 we report the effective exponent $\hat{\tau}_{\mathrm{exp},R_g^2}(t;s)$ for $N=300$, $d=2$, $s=2000$. It increases with $t$ and becomes constant within error bars for $t\gtrsim106\,000$. We have taken our estimate at $t\approx130\,000\approx3\,\tau_{\mathrm{exp},R_g^2}$. The same analysis has been done for all observables and all values of $N$. The results are reported in Table I.

We have determined the dynamic exponent $z_{\mathrm{exp},A}$ by fitting the results of Table I with the ansatz

$$\tau_{\mathrm{exp},A}=B_A N^{z_{\mathrm{exp},A}}. \tag{20}$$

The results are reported in Table II. Since we only have three values of $N$, we cannot study the effect of corrections to scaling and thus we cannot determine the systematic error on our results. However, an indication can be obtained by comparing the results for the three radii. Indeed, one expects these three observables to have the same dynamic exponent. In two dimensions, $z_{\mathrm{exp},R_e^2}$ differs significantly from the estimates for the other radii, indicating the presence of large corrections to scaling. Such conclusion is confirmed by the scaling analysis that will be reported below: as we shall see, the results of Table II in two dimensions are effective exponents that are expected to decrease as larger values of $N$ are included in the fit. Of course, it is possible that also $z_{\mathrm{exp},\mathcal{E}}$ is affected by large corrections to scaling. However, the scaling analysis confirms the result for $z_{\mathrm{exp},\mathcal{E}}$, thus showing that the scaling corrections are important for the radii only.

In three dimensions, there is no evidence of large scaling corrections. Indeed, the exponents $z_{\mathrm{exp}}$ for the three radii agree within error bars. The dynamic exponent for the energy is lower than that for the radii. However, the difference is small and it is not clear if it is real or just the result of neglected corrections to scaling.

TABLE IV. Dynamic exponent $z_{\mathrm{int}}$ for the EER algorithm in two and three dimensions, obtained by fitting $\tau_{\mathrm{int}}=BN^{z_{\mathrm{int}}}$. The number of degrees of freedom of the fit is 1.

| $d$ | | $\tau_{\mathrm{int},R_g^2}$ | $\tau_{\mathrm{int},R_e^2}$ | $\tau_{\mathrm{int},R_m^2}$ | $\tau_{\mathrm{int},\mathcal{E}}$ |
|---|---|---|---|---|---|
| | $z_{\mathrm{int}}$ | $2.227\pm0.002$ | $2.182\pm0.002$ | $2.198\pm0.002$ | $1.673\pm0.001$ |
| 2 | $B$ | $0.1100\pm0.0010$ | $0.0956\pm0.0008$ | $0.0856\pm0.0008$ | $0.392\pm0.002$ |
| | $\chi^2$ | 0.660 | 1.04 | 0.054 | 1470 |
| | $z_{\mathrm{int}}$ | $2.088\pm0.002$ | $2.052\pm0.002$ | $2.062\pm0.002$ | $1.681\pm0.001$ |
| 3 | $B$ | $0.1820\pm0.0020$ | $0.1386\pm0.0012$ | $0.1338\pm0.0010$ | $0.392\pm0.002$ |
| | $\chi^2$ | 0.804 | 0.625 | 0.191 | 851 |

TABLE V. Dynamic exponents $a$ and $b$ for the EER algorithm in two and three dimensions.

| $d$ | | $R_g^2$ | $R_e^2$ | $R_m^2$ | $\mathcal{E}$ |
|---|---|---|---|---|---|
| 2 | $b$ | $2.21\pm0.02$ | $2.20\pm0.02$ | $2.22\pm0.02$ | $2.14\pm0.02$ |
| | $a$ | $0.0010\pm0.0010$ | $0.0025\pm0.0020$ | $0.002\pm0.002$ | $0.285\pm0.025$ |
| 3 | $b$ | $2.085\pm0.015$ | $2.068\pm0.015$ | $2.085\pm0.015$ | $2.030\pm0.025$ |
| | $a$ | $0.0012\pm0.0010$ | $0.0025\pm0.0025$ | $0.0015\pm0.0015$ | $0.210\pm0.020$ |

Then, we have computed the integrated autocorrelation times by using the self-consistent windowing method with $c=15$, cf. Eq. (13). The results are reported in Table III.

For the radii, $\tau_{\exp,R^2}\sim 1-2\,\tau_{\mathrm{int},R^2}$ and thus the choice $c=15$ should be rather conservative. For the energy, $c=15$ corresponds to $1.3\tau_{\exp,\mathcal{E}}\lesssim M\lesssim 4\,\tau_{\exp,\mathcal{E}}$ in two dimensions and to $2\,\tau_{\exp,\mathcal{E}}\lesssim M\lesssim 5\,\tau_{\exp,\mathcal{E}}$ in three dimensions for our values of $N$ [$M$ is the cutoff defined in Eq. (13)]. Such values of $M$ can give rise, at least for $N=1000$, to a systematic underestimate of $\tau_{\mathrm{int},\mathcal{E}}$. For our choice of $c$ and for $N=1000$, $\rho_{\mathcal{E}\mathcal{E}}(M)\approx(7.2\pm1.5)10^{-4}$ and $(4.9\pm1.0)10^{-4}$ in two and three dimensions, respectively. Therefore, assuming a pure exponential behavior for $t>M$, the neglected contribution should be of order $320\pm60$ in $d=2$ and $150\pm30$ in $d=3$. The correction is quite small, but larger than the quoted error bars: the correct errors are at least larger by a factor of 5 (2) in two (three) dimensions.

The results for $\tau_{\mathrm{int},A}$ have been fitted with the ansatz

$$\tau_{\mathrm{int},A}=B_A N^{z_{\mathrm{int},A}}. \tag{21}$$

The results are reported in Table IV.

The error bars are purely statistical and, as in the case of $z_{\exp}$, large systematic errors may be present. We expect the quantities that measure the walk size to have the same dynamic exponent $z_{\mathrm{int}}$. Thus, both in two and three dimensions, the reported errors are largely underestimated. More conservative estimates are

$$z_{\mathrm{int},R^2}=2.20\pm0.03, \quad d=2,$$
$$z_{\mathrm{int},R^2}=2.07\pm0.02 \quad d=3. \tag{22}$$

The fit for the energy has a very large $\chi^2$. There are two reasons for this. First, the statistical errors are underestimated, as we already discussed. Second, there may be large—compared to the tiny statistical errors—corrections to scaling. For these reasons, the errors quoted in Table IV for $z_{\mathrm{int},\mathcal{E}}$ should not be taken seriously. A more realistic estimate is obtained by multiplying the errors by $\sqrt{\chi^2}$, which gives an error of $\pm0.04$ on the exponent in both two and three dimensions. Such error is more realistic and indeed is close to the error we quoted for the radii, cf. Eq. (22).

The dynamic critical exponents can also be determined by analyzing the scaling behavior of the autocorrelation function, see Eq. (17), i.e., by determining $a$ and $b$ so that $N^{ab}\hat{\rho}_{AA}(t)$ is a universal function of $tN^{-b}$, independent of $N$. In Table V, we report the values of $a$ and $b$ for which a collapse of the autocorrelation functions is observed. In Fig. 5, we show the corresponding plots for $R_g^2$ and $\mathcal{E}$ in two dimensions.

For the energy we observe a very good collapse, while for the radii the scaling behavior deteriorates as $tN^{-b}$ increases. Since the vertical scale changes by several orders of magnitude, the deviations are somewhat difficult to observe and this makes difficult to set the errors on $a$ and $b$. For this purpose, we found more useful to consider, instead of $N^{ab}\hat{\rho}_{AA}(t)$, the quantity

$$\tau_{\mathrm{scal},A}(t;N)=-\frac{tN^{-b}}{\ln(N^{ab}\hat{\rho}_{AA}(t))} \tag{23}$$

that is also a universal function of $tN^{-b}$ in the scaling limit and that scales as $\tau_{\exp,A}N^{-b}$ for $tN^{-b}\to\infty$.

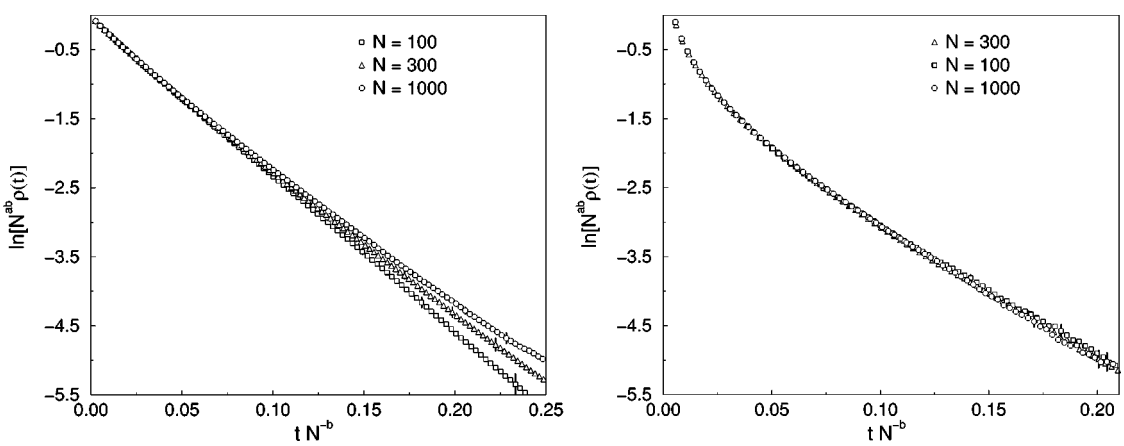


FIG. 5. Dynamic scaling analysis for the EER algorithm in two dimensions: plots of $\ln[N^{ab}\hat{\rho}_{AA}(t)]$ vs $tN^{-b}$. Left frame: $A=R_g^2$, $a=0.001$, $b=2.21$; right frame: $A=\mathcal{E}$, $a=0.285$, $b=2.14$.

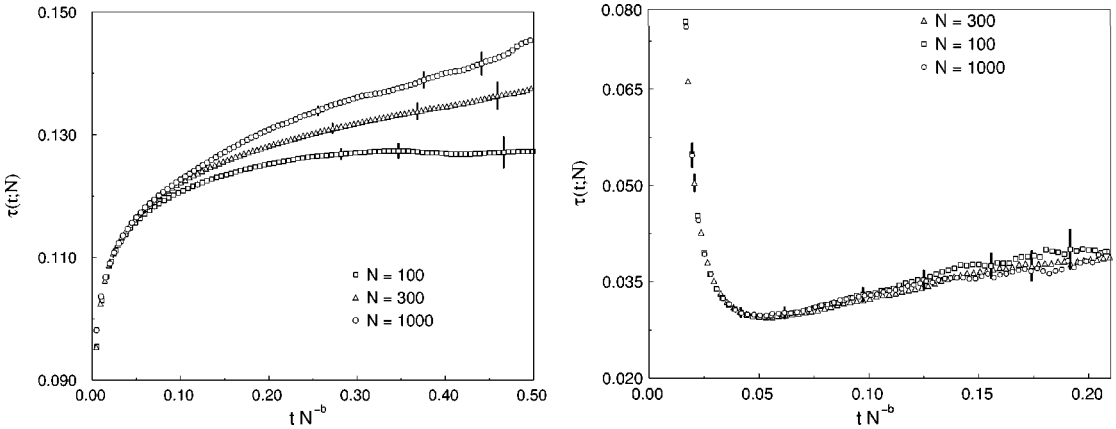


FIG. 6. Dynamic scaling analysis for the EER algorithm in two dimensions: plots of $\tau_{\mathrm{scal},A}(t;N)$ vs $tN^{-b}$. Left frame: $A=R_g^2$, $a=0.001$, $b=2.21$; right frame: $A=\mathcal{E}$, $a=0.285$, $b=2.14$.

In Fig. 6, we report the quantity $\tau_{\mathrm{scal},A}(t;N)$ for $R_g^2$ and $\mathcal{E}$. The energy shows a very good scaling behavior while the scaling is quite poor for $R_g^2$, although it improves as $N$ increases: the data for $N=100$ and $N=300$ overlap up to $tN^{-b}\approx 0.05$, while the data for $N=300$ and $N=1000$ overlap up to $tN^{-b}\approx 0.09$.

In three dimensions, all observables show a very good scaling behavior, as it can be seen from Fig. 7. In all cases, the results for the three values of $N$ fall onto a single curve.

From the results of Table V we can compute the exponents $z_{\mathrm{exp}}$ and $z_{\mathrm{int}}$, cf. Eqs. (18) and (19), and compare them with the previous results. In three dimensions, the estimates of $z_{\mathrm{exp}}$ obtained from the scaling analysis are in perfect agreement with those of Table II. In two dimensions instead, only $z_{\mathrm{exp},\mathcal{E}}$ is compatible with the results of Table II. The estimates of $z_{\mathrm{exp}}$ for the radii obtained from the scaling analysis are significantly lower than those obtained from fitting the autocorrelation times. The origin of the discrepancy can be understood from Fig. 6. The exponential time is determined by the large-$t$ behavior of $\rho_{AA}(t)$ and in practice by the behavior in the region in which $t\approx 3\tau_{\mathrm{exp},R^2}$, see Fig. 4, which corresponds approximately to $tN^{-b}\approx 0.44$. But in this region there is no scaling, and thus the corresponding $\tau_{\mathrm{exp},R^2}$ do not scale as $N^{z_{\mathrm{exp},R^2}}$. For this reason, we believe the estimates of Table II to be grossly in error. Note also that the estimate we obtain in the scaling analysis, $z_{\mathrm{exp},R^2}\approx 2.21$, is compatible with $z_{\mathrm{exp},R^2}\approx z_{\mathrm{int},R^2}$, a relation that is expected to be true, since the radii are strongly coupled to the slowest modes of the dynamics.

Then, we can compute $z_{\mathrm{int},A}$. For the radii, we always have $a\approx 0$, so that $z_{\mathrm{int},R^2}\approx z_{\mathrm{exp},R^2}$ as expected. This confirms the results of Table IV. For the energy, we have instead $a\neq 0$. Using Eq. (19), we obtain

$$z_{\mathrm{int},\mathcal{E}}=1.53\pm 0.06, \quad d=2, \tag{24}$$

$$z_{\mathrm{int},\mathcal{E}}=1.60\pm 0.05, \quad d=3. \tag{25}$$

These results are in reasonable agreement with those reported in Table IV if one takes into account that, as we discussed, the error on those results is of order 0.04.

In conclusion, putting the results of the different analyses together, we obtain in two dimensions:

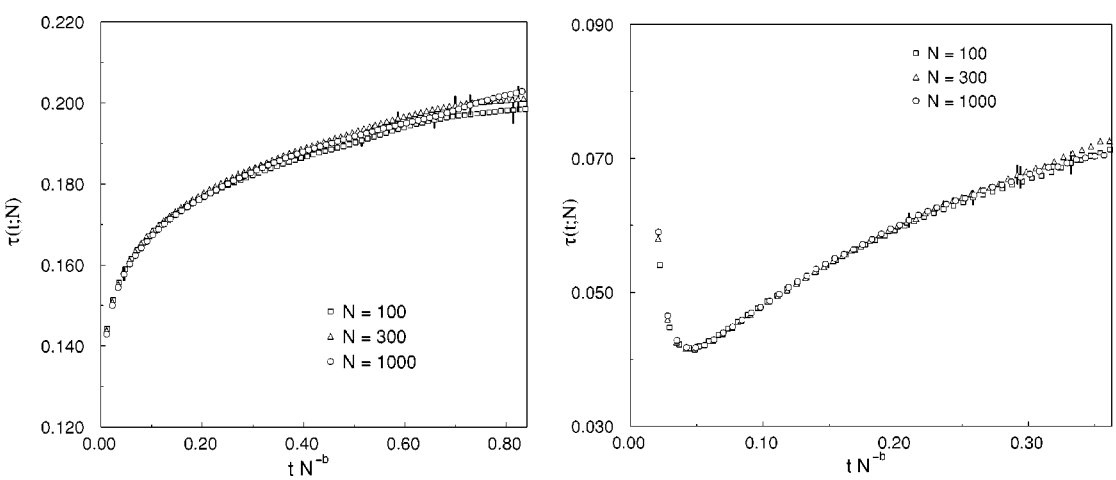


FIG. 7. Dynamic scaling analysis for the EER algorithm in three dimensions: plots of $\tau_{\mathrm{scal},A}(t;N)$ vs $tN^{-b}$. Left frame: $A=R_g^2$, $a=0.0012$, $b=2.085$; right frame: $A=\mathcal{E}$, $a=0.210$, $b=2.03$.

TABLE VI. Exponential autocorrelation times for the KER algorithm in two and three dimensions. "iter." is the number of iterations.

| $N$ | iter. | $\tau_{\exp,R_g^2}$ | $\tau_{\exp,R_e^2}$ | $\tau_{\exp,R_m^2}$ |
|---|---|---|---|---|
| 100 | $2.4\times10^{11}$ | $37600\pm160$ | $38000\pm160$ | $38620\pm100$ |
| 300 | $8.8\times10^{11}$ | $918000\pm8000$ | $958000\pm8000$ | $972000\pm8000$ |
| 700 | $1.9\times10^{12}$ | $11475000\pm315000$ | $11610000\pm315000$ | $11250000\pm225000$ |

$$z_{\exp,R^2}=z_{\mathrm{int},R^2}=2.2\pm0.1,$$

$$z_{\exp,\mathcal{E}}=2.15\pm0.05,$$

$$z_{\mathrm{int},\mathcal{E}}=1.60\pm0.10. \tag{26}$$

In three dimensions we have

$$z_{\exp,R^2}=z_{\mathrm{int},R^2}=2.07\pm0.05,$$

$$z_{\exp,\mathcal{E}}=2.05\pm0.05,$$

$$z_{\mathrm{int},\mathcal{E}}=1.65\pm0.05. \tag{27}$$

The errors are such to include the results of all analyses.

Note that $z_{\mathrm{int},\mathcal{E}}<z_{\exp,\mathcal{E}}$ for the EER dynamics. This may be understood as follows. The energy fluctuations are essentially due to two causes. First, there are fluctuations due to local changes of the walk. These fluctuations are fast since these are due to local and bilocal moves. Then, there are fluctuations due to changes of the global structure of the walk. Indeed, there are contributions to the energy that are due to groups of monomers that are far apart along the walk but that are near in position space. Such contributions vary slowly, typically as $\tau_{\exp,R^2}$, and are the origin of the fact that $z_{\exp,\mathcal{E}}\approx z_{\exp,R^2}$. However, these contributions are very small, and thus give rise to tiny fluctuations that are negligible when considering integrated quantities. Therefore, $z_{\mathrm{int},\mathcal{E}}<z_{\exp,\mathcal{E}}$.

All results we have discussed up to now refer to simulations with $p=0.5$ and with the first version of the reptation move. These choices are of no relevance for the critical exponents, but they have of course a strong influence on the amplitudes. We have thus tried to see the changes in the dynamics due to a variation of $p$ and to a change of the reptation move. To check the role of $p$, we have performed simulations with $p=0.1$ and $p=0.9$ with walks of length $N=100$ in two dimensions. We find: for $p=0.9$, $\tau_{\mathrm{int},R_e^2}=2184\pm32$ and $\tau_{\mathrm{int},\mathcal{E}}=1200\pm13$; for $p=0.1$, $\tau_{\mathrm{int},R_e^2}=8740\pm260$ and $\tau_{\mathrm{int},\mathcal{E}}=1181\pm13$. This should be compared with the results of Table III, $\tau_{\mathrm{int},R_e^2}\approx3110$ and $\tau_{\mathrm{int},\mathcal{E}}\approx862$. Thus, by increasing $p$, there is a significant speed up of the dynamics of the radii—this should be expected, since reptation moves are essentially the only ones that change the position of the end point and are thus those that control the slowest modes of the dynamics. Thus, for noninteracting SAWs, for which the energy is not an interesting observable, $p$ close to one—but not $p=1$, otherwise ergodicity is lost—is a good choice for a fast dynamics. On the other hand, the dynamics of the energy becomes slower both for $p=0.1$ and for $p=0.9$. The fact that $\tau_{\mathrm{int},\mathcal{E}}$ is larger for $p=0.9$ is easy to understand. Indeed, by increasing $p$ we decrease the probability of performing L0 and B22 moves that should be the most important ones for the energy. However, it is clear that reptation moves are also relevant for the energy, since for $p=0.1$, $\tau_{\mathrm{int},\mathcal{E}}$ is also larger. Apparently, for small $p$ the relevant quantity for the dynamics of the energy is the number of

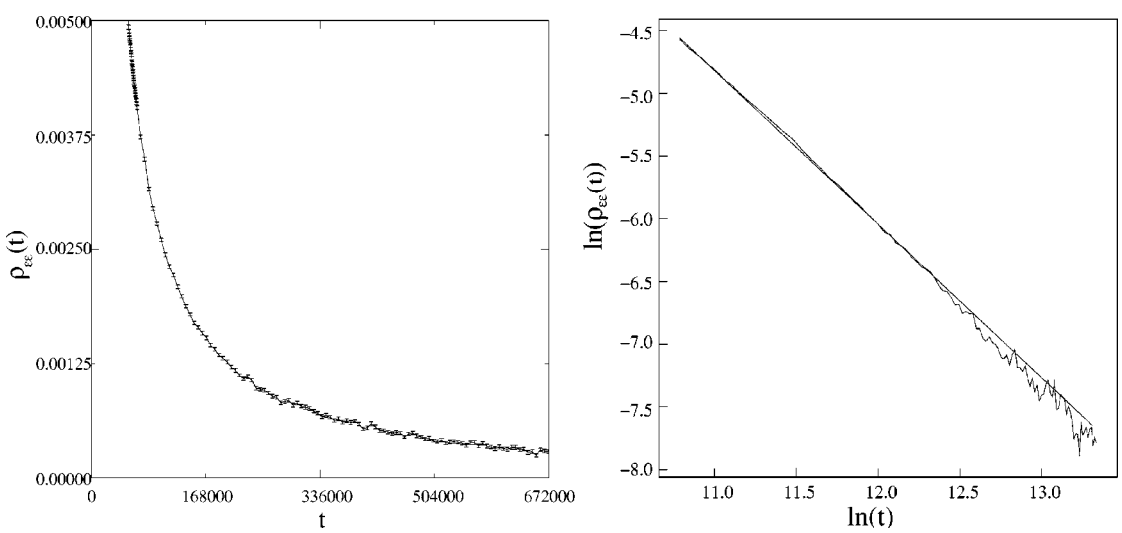


FIG. 8. Autocorrelation function $\hat{\rho}_{\mathcal{E}\mathcal{E}}(t)$ for the KER algorithm in two dimensions. Here $N=300$. The straight line in the right frame corresponds to $Bt^{-\alpha}$, $B=5100$, $\alpha=1.29$.

TABLE VII. Dynamic exponent $z_{\rm exp}$ for the KER algorithm in two and three dimensions, obtained by fitting $\tau_{\rm exp}=BN^{z_{\rm exp}}$. The number of degrees of freedom of the fit is 1.

| | $\tau_{{\rm exp},R_g^2}$ | $\tau_{{\rm exp},R_e^2}$ | $\tau_{{\rm exp},R_m^2}$ |
|---|---|---|---|
| $z_{\rm exp}$ | $2.92\pm0.01$ | $2.94\pm0.01$ | $2.93\pm0.01$ |
| $B$ | $0.054\pm0.002$ | $0.050\pm0.002$ | $0.054\pm0.002$ |
| $\chi^2$ | 3.77 | 0.034 | 2.46 |

successful moves, irrespective of the type. Indeed, using the results of Sec. 1 and Sec. 2 of the Appendix we find $\tau_{{\rm int},\mathcal{E}}\approx600$ successful iterations both for $p=0.5$ and $p=0.1$.

We have also tested the second version of the reptation algorithm, see Sec. 2 of the Appendix. For random walks, this implementation gives $\tau\sim N$ compared to $\tau\sim N^2$ of the first version. For the SAW, the two versions are expected to have the same critical exponents, but the second one should be faster. We have performed a simulation with $p=0.5$ in two dimensions, finding $\tau_{{\rm int},R_e^2}=510\pm4$ and $\tau_{{\rm int},\mathcal{E}}=299.8\pm1.6$. These estimates are sensibly smaller than those reported in Table III. For $R_e^2$ the dynamics is faster by a factor of 6, and for $\mathcal{E}$ by a factor of 3. Clearly, the second implementation is the most efficient one and all our simulations should have used it. Unfortunately, we thought of this second version only when all simulations were completed.

## VI. THE KER DYNAMICS IN TWO DIMENSIONS

The second dynamics we have analyzed is the KER algorithm in which end-end reptation moves BEE are replaced by kink-end reptation moves BKE. It turns out that this dynamics is much slower than the EER one, and thus we have limited our analysis to shorter walks, $N=100,300,700$, to two dimensions, and to noninteracting SAWs, i.e. $\beta=0$. We set $p=0.5$. Again, we measured three radii and the energy. The static results agree with those obtained by using the EER dynamics and discussed in the preceding section and with the results of Ref. [47].

As in the preceding section, we have first determined the exponential autocorrelation times by studying the large-time behavior of the effective exponents $\hat{\tau}_{{\rm exp},A}(t;s)$, see Sec. IV. The results for the radii are reported in Table VI. We have not been able to determine the exponential autocorrelation time for the energy $\mathcal{E}$. Indeed, for the values of $t$ for which $\rho_{\mathcal{E}\mathcal{E}}(t)$ is not zero within statistical errors, $\rho_{\mathcal{E}\mathcal{E}}(t)$ has a power-law behavior, i.e., $\rho_{\mathcal{E}\mathcal{E}}(t)\sim t^{-\alpha}$, with $\alpha\approx1$–1.3. This can clearly be seen from Fig. 8 where we report $\rho_{\mathcal{E}\mathcal{E}}(t)$ for $N=300$.

The results for the exponential autocorrelation times are fitted with the ansatz (20), obtaining the results reported in Table VII. As before, we cannot perform a systematic analysis of the scaling corrections. However, it is important to notice that the estimates for the three radii agree within error bars. This confirms the correctness of the quoted error bars and gives the final estimate

$$z_{{\rm exp},R^2}=2.93\pm0.02. \tag{28}$$

This estimate is significantly higher than that for the EER dynamics. The origin of such a large difference is unclear, since it is difficult to see any difference between BEE and BKE moves. Naively, one would have expected a BKE move to be equivalent to two BEE moves together with a B22 move. Since all moves have a finite probability of success as $N\to\infty$, see Appendix, one would have expected a difference by a constant factor, and thus the same critical exponents. Such a naive expectation is not true, since the exponents are clearly different.

We have then determined the integrated autocorrelation times. For the radii we have used the self-consistent windowing method of Sec. IV, using $c=15$. The results are reported in Table VIII. Since $\tau_{{\rm exp},R^2}\sim3\tau_{{\rm int},R^2}$, the choice $c=15$ should be enough to avoid systematic errors. Instead, the autocorrelation function of the energy decreases rapidly and it has a very long tail. In this case, we have chosen a much larger valus of $c$, $c=200$, obtaining the results that are reported in Table VIII as $\tau_{{\rm int},\mathcal{E}}({\rm nt})$. In spite of $c$ being such a large number, the cutoff value $M$, cf. Eq. (13), is still well within the region in which the function decays as a power law. For instance, for $N=300$, $M=670\,000$ ($\ln M\approx13.4$) and $\rho(M)\approx3.4\times10^{-4}$, see Fig. 8. This should be expected since the cutoff $M$ satisfies $M\lesssim\tau_{{\rm exp},R^2}\approx10^6$. More precisely, $M\approx3.3\tau_{{\rm exp},R^2}$, $M\approx0.7\tau_{{\rm exp},R^2}$, and $M\approx0.14\tau_{{\rm exp},R^2}$ approximately for $N=100,300,700$. Therefore, we expect a sizable contribution from the tail of the autocorrelation function, at least for $N=300,700$. To take it into account, we use Eq.

TABLE VIII. KER algorithm in two dimensions: integrated autocorrelation times and dynamic critical exponents $z_{\rm int}$, obtained by fitting $\tau_{\rm int}=BN^{z_{\rm int}}$. The number of degrees of freedom of the fit is 1. For the energy $\mathcal{E}$, we report two estimates: (nt) is obtained by using the self-consistent windowing method with $c=200$, while (wt) is the result obtained including the tail contribution in the manner of Li *et al.* (Ref. [47]).

| $N$ | $\tau_{{\rm int},R_g^2}$ | $\tau_{{\rm int},R_e^2}$ | $\tau_{{\rm int},R_m^2}$ | $\tau_{{\rm int},\mathcal{E}}$(nt) | $\tau_{{\rm int},\mathcal{E}}$(wt) |
|---|---|---|---|---|---|
| 100 | $15632\pm30$ | $20974\pm48$ | $27528\pm72$ | $847.5\pm0.4$ | $847.5\pm0.4$ |
| 300 | $341030\pm1640$ | $462700\pm2600$ | $648500\pm4300$ | $3402.6\pm1.6$ | $3484\pm4$ |
| 700 | $3906500\pm43800$ | $5325000\pm70000$ | $7942000\pm127000$ | $9269.0\pm5.1$ | $10948\pm90$ |
| $z_{\rm int}$ | $2.820\pm0.005$ | $2.830\pm0.004$ | $2.890\pm0.006$ | $1.2330\pm0.0004$ | $1.289\pm0.0011$ |
| $B$ | $0.0360\pm0.0007$ | $0.0464\pm0.0010$ | $0.0458\pm0.0012$ | $2.920\pm0.006$ | $0.808\pm0.005$ |
| $\chi^2$ | 18.5 | 11.8 | 11.8 | 4197 | 41.7 |

TABLE IX. Dynamic exponents $a$ and $b$ for the KER algorithm in two dimensions. For the energy, we have fixed $b=2.93\pm0.04$ and determined the corresponding $a$.

| | $R_g^2$ | $R_e^2$ | $R_m^2$ | $\mathcal{E}$ |
|---|---|---|---|---|
| $b$ | $2.89\pm0.03$ | $2.92\pm0.02$ | $2.92\pm0.02$ | $[2.93\pm0.04]$ |
| $a$ | $0.015\pm0.015$ | $0.020\pm0.015$ | $0.015\pm0.010$ | $0.670\pm0.015$ |

(15), where for $\tau_{\exp,\mathcal{E}}$ we take the average $\tau_{\exp,R^2}$ of the radii. For $N=300$ the correction is of 2.5% [2.4% if we approximate $\rho_{\mathcal{E}\mathcal{E}}(t)\approx Bt^{-1.3}$ as obtained from the fit] and for $N=700$ of 20.3% [18.1% if we approximate $\rho_{\mathcal{E}\mathcal{E}}(t)\approx Bt^{-1.1}$ as obtained from the fit]. The results are reported in Table VIII as $\tau_{\mathrm{int},\mathcal{E}}(\mathrm{wt})$. The reported error is obtained by summing 20% of the contribution of the tail to the original error. This is an *ad hoc* prescription which can be shown to work reasonably in the exactly soluble case of the pivot algorithm for the random walk.

The results for the autocorrelation times have been fitted with the ansatz (21) in order to obtain $z_{\mathrm{int}}$. For the radii, the quality of the fits is quite poor, with a $\chi^2$ of approximately 10–20. Moreover, the estimates do not agree within error bars. There are, therefore, corrections to scaling larger than the very tiny statistical errors. By requiring $z_{\mathrm{int},R^2}$ to coincide for these three quantities, we obtain finally

$$z_{\mathrm{int},R^2}=2.85\pm0.06, \tag{29}$$

which includes all estimates and is compatible with the expectation $z_{\mathrm{int},R^2}=z_{\exp,R^2}$.

Fits of $\tau_{\mathrm{int},\mathcal{E}}$ are characterized by a very large $\chi^2$ and give $z_{\mathrm{int},\mathcal{E}}\approx1.2$–$1.3$, much smaller than $z_{\mathrm{int},R^2}$. As in the EER algorithm, the dynamics of the energy is much faster than that of the radii. Note that $z_{\mathrm{int},\mathcal{E}}$ is also significantly lower that the corresponding exponent for the EER algorithm. Again, it is quite difficult to understand intuitively why this happens.

The results reported above are confirmed by a scaling analysis using Eq. (17). The results for the radii are reported in Table IX. The exponent $a$ is compatible with zero and $z_{\exp,R^2}=b=2.91\pm0.03$, in agreement with the estimate (28).

Since $\rho_{\mathcal{E}\mathcal{E}}(t)\sim Bt^{-\alpha}$ for the values of $t$ we can investigate, we cannot determine $a$ and $b$ independently. Thus, we have assumed $z_{\exp,\mathcal{E}}=z_{\exp,R^2}$ and then used $b=2.93\pm0.04$, cf. Eq. (28)—to be conservative, we have doubled the error. Correspondingly, we obtain $a=0.670\pm0.015$ and $z_{\mathrm{int},\mathcal{E}}=0.97\pm0.05$, which is somewhat lower than the estimates of Table VIII. One may think that this is due to our assumption $z_{\exp,\mathcal{E}}=z_{\exp,R^2}$, while there is some evidence from the analysis of the EER dynamics that $z_{\exp,\mathcal{E}}<z_{\exp,R^2}$. However, this does not explain the difference, since if $z_{\exp,\mathcal{E}}$ decreases, also $z_{\mathrm{int},\mathcal{E}}$ decreases. In order to obtain $z_{\mathrm{int},\mathcal{E}}=1.3$, one should take $z_{\exp,\mathcal{E}}=b=3.35$, which is much too large. Therefore, the difference should be taken as an indication of the scaling corrections.

TABLE XI. Dynamic exponent $z_{\exp}$ for the EER algorithm in two dimensions at the $\theta$ point, obtained by fitting $\tau_{\exp}=BN^{z_{\exp}}$. The number of degrees of freedom of the fit is 2.

| | $\tau_{\exp,R_g^2}$ | $\tau_{\exp,R_e^2}$ | $\tau_{\exp,R_m^2}$ | $\tau_{\exp,\mathcal{E}}$ |
|---|---|---|---|---|
| $z_{\exp}$ | $2.318\pm0.004$ | $2.275\pm0.003$ | $2.300\pm0.004$ | $2.313\pm0.004$ |
| $B$ | $0.126\pm0.006$ | $0.148\pm0.004$ | $0.128\pm0.005$ | $0.116\pm0.006$ |
| $\chi^2$ | 2.01 | 3.64 | 1.24 | 0.78 |

In conclusion, the KER dynamics has a different critical behavior with respect to the EER dynamics. For the critical exponents we have

$$z_{\exp,R^2}=z_{\mathrm{int},R^2}=2.90\pm0.05, \tag{30}$$

$$z_{\mathrm{int},\mathcal{E}}=1.0\pm0.3. \tag{31}$$

## VII. THE EER DYNAMICS AT THE $\theta$ POINT IN TWO DIMENSIONS

Bilocal algorithms are of interest for applications in constrained geometries and in the presence of strong interactions where nonlocal algorithms are inefficient.

In this section, we study the dynamic behavior of the EER algorithm at the $\theta$ point in two dimensions, by setting $\beta=\beta_\theta=0.665$—we have used the estimate of Ref. [42]. Here, we have studied longer walks than before, $N=100,800,1600,3200$, with large statistics, see Table X.

We have performed the same analyses we have presented in the preceding sections. First, we determined the exponential autocorrelation times, see Table X, and the exponents $z_{\exp,A}$, see Table XI. Clearly, the statistical errors are too small. Indeed, we expect $z_{\exp,A}$ to be the same for all observables—including the energy, that should be strongly coupled to the slowest modes at the $\theta$ point—and this does not happen with the quoted error bars. By direct comparison of all estimates, we obtain the more conservative result

$$z_{\exp,\mathcal{E}}=z_{\exp,R^2}=2.30\pm0.03, \tag{32}$$

where the error is such to include all estimates.

TABLE X. Exponential autocorrelation times for the EER algorithm in two dimensions at the $\theta$ point. "iter." is the number of iterations.

| $N$ | iter. | $\tau_{\exp,R_g^2}$ | $\tau_{\exp,R_e^2}$ | $\tau_{\exp,R_m^2}$ | $\tau_{\exp,\mathcal{E}}$ |
|---|---|---|---|---|---|
| 100 | $5.84\times10^{10}$ | $5120\pm70$ | $5220\pm60$ | $5170\pm40$ | $4856\pm44$ |
| 800 | $6.28\times10^{11}$ | $609600\pm15000$ | $606000\pm10000$ | $620000\pm8000$ | $594200\pm9000$ |
| 1600 | $1.81\times10^{12}$ | $3165000\pm22000$ | $2840000\pm20000$ | $3020000\pm20000$ | $2936000\pm24000$ |
| 3200 | $1.12\times10^{13}$ | $15838000\pm76000$ | $13880000\pm50000$ | $14990000\pm50000$ | $14656000\pm50000$ |

TABLE XII. EER algorithm in two dimensions at the $\theta$ point: integrated autocorrelation times and dynamic critical exponents $z_{\rm int}$, obtained by fitting $\tau_{\rm int}=BN^{z_{\rm int}}$. The number of degrees of freedom of the fit is 2.

| $N$ | $\tau_{{\rm int},R_g^2}$ | $\tau_{{\rm int},R_e^2}$ | $\tau_{{\rm int},R_m^2}$ | $\tau_{{\rm int},\mathcal{E}}$ |
|---|---|---|---|---|
| 100 | $4520\pm10$ | $3166.2\pm5.8$ | $3082.8\pm5.4$ | $2504.4\pm4.0$ |
| 800 | $559500\pm4100$ | $362300\pm2100$ | $357900\pm2100$ | $222800\pm1000$ |
| 1600 | $2890400\pm28300$ | $1779500\pm13700$ | $1778000\pm13600$ | $1029500\pm6000$ |
| 3200 | $13953000\pm120000$ | $8630000\pm59000$ | $8698000\pm59000$ | $4185000\pm20000$ |
| $z_{\rm int}$ | $2.321\pm0.002$ | $2.282\pm0.002$ | $2.291\pm0.002$ | $2.1510\pm0.0011$ |
| $B$ | $0.1020\pm0.0013$ | $0.0864\pm0.0008$ | $0.0800\pm0.0010$ | $0.1260\pm0.0008$ |
| $\chi^2$ | 9.0 | 1.22 | 3.73 | 149 |

We have analogously determined the integrated autocorrelation times using the self-consistent windowing method with $c=15$. The results for $\tau_{{\rm int},A}$ are reported in Table XII. Notice that in this case the integrated autocorrelation times for the energy are close to those of the radii, as it should be expected, since at the $\theta$ point also the energy is a "slow" variable. In all cases, $\tau_{{\rm exp},A}\sim1-3\,\tau_{{\rm int},A}$ and thus the choice $c=15$ should give a small systematic error due to the truncation of the autocorrelation functions.

The integrated autocorrelation times have been fitted with the ansatz $BN^{z_{\rm int}}$, in order to compute $z_{{\rm int},A}$. The results are reported in Table XII. In all cases, the purely statistical errors we have reported are too small. For the radii, the exponent $z_{\rm int}$ should be the same, and thus the error is at least a factor of ten larger. Comparing the estimates of Table XII, we arrive at the final result

$$z_{{\rm int},R^2}=2.30\pm0.03, \tag{33}$$

which, by comparing with Eq. (32), gives $z_{{\rm int},R^2}=z_{{\rm exp},R^2}$, as expected.

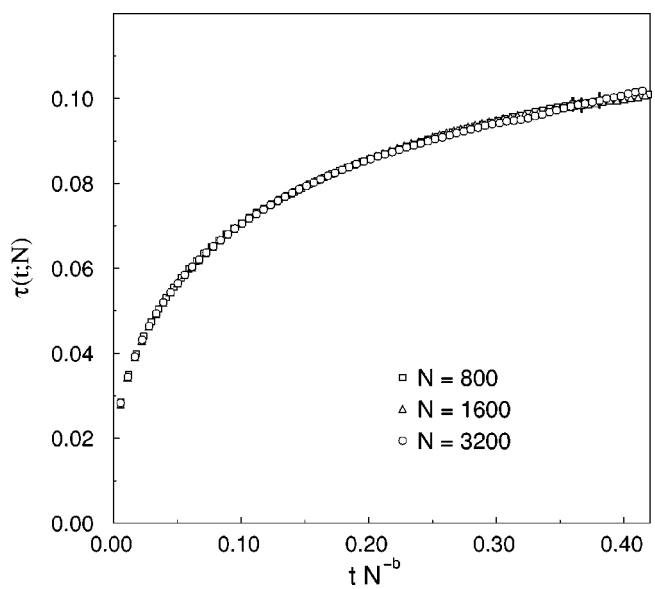


FIG. 9. Dynamic scaling analysis for the EER algorithm in two dimensions at the $\theta$ point: plots of $\tau_{{\rm scal},R_m^2}(t;N)$ vs $tN^{-b}$. Here $a=0.0015$, $b=2.31$.

The result for $\mathcal{E}$ is somewhat lower, but the very large $\chi^2$ indicates that corrections to scaling are significant. In order to see if there is a systematic trend we have determined an effective $z_{{\rm int},\mathcal{E}}$, by computing

$$\hat{z}_{{\rm int},\mathcal{E}}(N_1,N_2)=\left[\ln\frac{\tau_{{\rm int},\mathcal{E}}(N_1)}{\tau_{{\rm int},\mathcal{E}}(N_2)}\right]\left(\ln\frac{N_1}{N_2}\right)^{-1}. \tag{34}$$

We obtain $\hat{z}_{{\rm int},\mathcal{E}}(100,800)=2.158(3)$, $\hat{z}_{{\rm int},\mathcal{E}}(800,1600)=2.208(15)$, $\hat{z}_{{\rm int},\mathcal{E}}(1600,3200)=2.023(15)$. It is difficult to observe a systematic trend, but in any case a systematic increase towards 2.30 seems to be excluded. On the contrary, the data seem to indicate that $z_{{\rm int},\mathcal{E}}$ decreases below the value of Table XII. Thus, also at the $\theta$ point we have $z_{{\rm int},\mathcal{E}}<z_{{\rm exp},\mathcal{E}}$, although the difference is much smaller than in the case $\beta=0$.

These results are confirmed by a scaling analysis. In Fig. 9, we report the scaling variable $\tau_{{\rm scal},R_m^2}(t;N)$. We observe a very good scaling behavior and correspondingly we are able to obtain quite reliable estimates of the critical exponents $a$ and $b$. The same good behavior is observed for all observables. The estimates of $a$ and $b$ are reported in Table XIII. For all observables, $b$ is compatible with the estimates of Table XI, confirming the estimate (32). For the radii, $a=0$, in agreement with Table XII. For the energy, $a$ is clearly nonvanishing, confirming that $z_{{\rm int},\mathcal{E}}<z_{{\rm exp},\mathcal{E}}$. Using Eq. (19), we have $z_{{\rm int},\mathcal{E}}=2.15\pm0.03$, which is in agreement with the previous results.

## VIII. CONCLUSIONS

The simulations we have presented show that the reptation dynamics is quite successful, even at the $\theta$ point. The values of $z$ we have found are only marginally higher than 2, which is the best possible behavior for a dynamics that in-

TABLE XIII. Dynamic exponents $a$ and $b$ for the EER algorithm in two dimensions at the $\theta$ point.

| | $R_g^2$ | $R_e^2$ | $R_m^2$ | $\mathcal{E}$ |
|---|---|---|---|---|
| $b$ | $2.315\pm0.015$ | $2.30\pm0.02$ | $2.31\pm0.02$ | $2.31\pm0.02$ |
| $a$ | $0.0015\pm0.0015$ | $0.002\pm0.002$ | $0.0015\pm0.0015$ | $0.07\pm0.01$ |

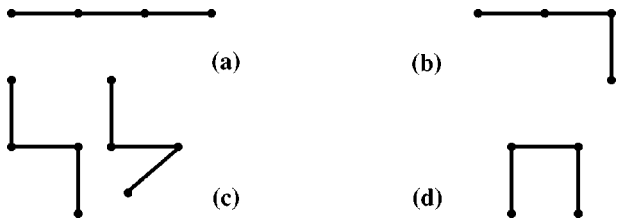


FIG. 10. Configurations of three consecutive links: (a) configuration of type I; (b) configuration of type L; (c) configuration of type S; (d) configuration of type U.

volves local and bilocal moves. Of course, for a practical implementation one may want to explore several variants that, although not changing the critical behavior, may still speed up the dynamics by a constant (large) factor. First of all, in practical implementations it is important to use the second version of the reptation dynamics (see Sec. 2 of the Appendix). Second, the B22 moves are quite rarely performed and in any case much less than the kink-end/end-kink moves. For instance, in two dimensions at $\beta=0$, B22 (BKE) moves are performed with probability 0.08 (0.13). Moreover, BKE moves appear to be quite successful in speeding up the dynamics of the energy, that is one of the slow variables in the presence of interactions. Therefore, in the compact regime an efficient dynamics can be obtained by mixing together: (i) the reptation move; (ii) the BKE move; (iii) purely local moves L0 and L1. A purely local algorithm that leaves the correct measure invariant can be obtained from that described in Sec. 1 of the Appendix by setting $p(0)=1/2$ in all dimensions and $p(22)=0$. In this case, it is convenient to include also crankshaft moves, see Sec. 4.1 of Ref. [16]. Such an implementation of the EER algorithm should be the method of choice for fixed $N$ simulations in the compact regime.

## APPENDIX: THE BASIC MOVES

In this appendix, we introduce the basic moves that we use in our simulation: (i) The kink-kink local/bilocal move; (ii) The reptation move; (iii) The kink-end/end-kink reptation move. In Ref. [16] it was shown that moves (iii) are enough to obtain an ergodic algorithm. In two dimensions one can limit oneself to consider only moves (i), but this algorithm is inefficient because of the slow motion of the endpoint. Reptation moves are never ergodic because of the possibility that the end points get trapped.

### 1. Kink-kink local/bilocal move

In this section we define the kink-kink local/bilocal move [16]. In order to describe the algorithm it is important to classify the possible configurations of three successive links (see Fig. 10): (1) the bonds have the same direction (I configuration); (2) two consecutive bonds have the same direction, while the third one is perpendicular to them (L configuration); (3) the first and the third bonds are perpendicular to the second one, and they are either parallel or perpendicular to each other (S configuration); (4) the first and the third bonds are perpendicular to the second one, and they are antiparallel to each other (U configuration). An iteration works as follows:

TABLE XIV. Proposal probability $p_{\rm pr}$ and probability $p_{\rm SA}$ that the proposed walk is self-avoiding for local (L0 and L1) and bilocal (B22) moves. We consider noninteracting SAWs in two and three dimensions.

| $d$ | $N$ | | L0, L1 | B22 |
|---|---|---|---|---|
| 2 | 100 | $p_{\rm pr}$ | 0.496 | 0.0952 |
| | | $p_{\rm SA}$ | 0.751 | 0.852 |
| | 300 | $p_{\rm pr}$ | 0.499 | 0.0963 |
| | | $p_{\rm SA}$ | 0.751 | 0.851 |
| | 700 | $p_{\rm pr}$ | 0.500 | 0.0966 |
| | | $p_{\rm SA}$ | 0.751 | 0.851 |
| | 1000 | $p_{\rm pr}$ | 0.500 | 0.0967 |
| | | $p_{\rm SA}$ | 0.751 | 0.851 |
| 3 | 100 | $p_{\rm pr}$ | 0.443 | 0.0850 |
| | | $p_{\rm SA}$ | 0.800 | 0.882 |
| | 300 | $p_{\rm pr}$ | 0.446 | 0.0864 |
| | | $p_{\rm SA}$ | 0.798 | 0.878 |
| | 1000 | $p_{\rm pr}$ | 0.447 | 0.0869 |
| | | $p_{\rm SA}$ | 0.798 | 0.877 |

*Step 1*. Choose a random site $i$ of the current walk $\omega$, $0\leqslant i\leqslant N$. If $i=N$, propose an L1 move and go to step 5.

*Step 2*. Determine the configuration of the subwalk $\omega[i-1,i+2]$. If $i=N-1$, we imagine adding a link $\Delta\omega(N)$ parallel to $\Delta\omega(N-1)$, so that the possible configurations are of type L and I. Analogously, if $i=0$, we imagine adding a link $\Delta\omega(-1)$ parallel to $\Delta\omega(0)$.

*Step 3*. Draw a random number $r$, uniformly distributed in [0,1]. Depending on the configuration of $\omega[i-1,i+2]$, do the following:

(1) I: If $r>(2d-2)p(22)$, perform a null transition and the iteration ends. Otherwise, go the next step.

(2) L: If $r>(2d-3)p(22)+p(0)$, perform a null transition and the iteration ends. If $(2d-3)p(22)<r<(2d-3)p(22)+p(0)$, propose an L0 move and go to step 5. Otherwise, go to the next step.

(3) S: If $r>(2d-4)p(22)+2p(0)$ perform a null transition and the iteration ends. If $(2d-4)p(22)<r<(2d-4)p(22)+2p(0)$ propose an L0 move: there are two possibilities which are chosen amongst randomly; then go to step 5. Otherwise, go to the next step.

(4) U: Go to the next step.

*Step 4*. Choose a second integer $j$ uniformly in the disjoint intervals, $-1\leqslant j\leqslant N$, $j\neq i-1,i,i+1$. If $j=-1,N$ make a null transition and the iteration ends. Otherwise, depending on the configuration of $\omega[i-1,i+2]$, do the following:

$\omega[i-1,i+2]$ is of type I, S, L: if $j=0$ or $j=N-1$, or if $\omega[j-1,j+2]$ is not of type U perform a null transition and the iteration ends. Otherwise, propose a B22 move, cutting the kink $\omega[j-1,j+2]$ and adding it to $\omega[i,i+1]$ in one of the possible directions [50]. Then, go to the next step.

TABLE XV. Proposal probability $p_{pr}$, probability $p_{SA}$ that the proposed walk is self-avoiding, and probability $p_{Met}$ that the proposed self-avoiding walk is accepted in the Metropolis test. For local (L0 and L1) and bilocal (B22) moves. We consider SAWs in two dimensions at the $\theta$ point.

| $N$ | | L0, L1 | B22 |
|---|---|---|---|
| 100 | $p_{pr}$ | 0.463 | 0.158 |
| | $p_{SA}$ | 0.429 | 0.525 |
| | $p_{Met}$ | 0.701 | 0.610 |
| 800 | $p_{pr}$ | 0.462 | 0.162 |
| | $p_{SA}$ | 0.394 | 0.416 |
| | $p_{Met}$ | 0.711 | 0.561 |
| 1600 | $p_{pr}$ | 0.462 | 0.163 |
| | $p_{SA}$ | 0.389 | 0.399 |
| | $p_{Met}$ | 0.714 | 0.556 |
| 3200 | $p_{pr}$ | 0.462 | 0.163 |
| | $p_{SA}$ | 0.385 | 0.388 |
| | $p_{Met}$ | 0.716 | 0.553 |

$\omega[i-1,i+2]$ is of type U: according to the configuration of $\omega[j-1,j+2]$ (if $j=0,N-1$ imagine adding links as before) do the following:

(1) $\omega[j-1,j+2]$ is of type I, S, L: If $r<c(\text{conf})p(22)$ (note that the random number $r$ appearing here is the same used in Step 3), propose a B22 move: cut the kink $\omega[i-1,i+2]$ and add it on top of $\omega[j,j+1]$ in a possible random direction [50], and then go to step 5. Otherwise, perform a null transition and the iteration ends. Here $c(\text{conf})=(2d-2)$, $(2d-4)$, $(2d-3)$ for conf = I, S, L, respectively.

(2) $\omega[j-1,j+2]$ is of type U: If $r<(2d-3)p(22)$, propose a B22 move: cut the kink $\omega[i-1,i+2]$ and add it on top of $\omega[j,j+1]$ in a possible random direction [50], and then go to step 5; if $(2d-3)p(22)<r<2(2d-3)p(22)$, propose a B22 move: cut the kink $\omega[j-1,j+2]$ and add it on top of $\omega[i,i+1]$ in a possible random direction, and then go to step 5. Otherwise, perform a null transition and the iteration ends.

*Step 5*. Check for self-avoidance. If the proposed new walk is self-avoiding keep it, otherwise perform a null transition.

*Step 6*. Compute the difference in energy between the old and the new walk and perform a Metropolis test.

The algorithm we have presented depends on the probabilities $p(0)$ and $p(22)$, that are the probabilities of L0 and B22 moves respectively. As discussed in Ref. [16], the fastest dynamics is obtained by setting $p(0)=p(22)=1/2$ in two dimensions, and $p(0)=1/3$, $p(22)=1/6$ in three dimensions.

TABLE XVI. Probability of the different moves for different $\beta$ and $d$.

| $d$ | $\beta$ | L0,L1 | B22 | Null |
|---|---|---|---|---|
| 2 | 0 | 0.38 | 0.08 | 0.54 |
| 3 | 0 | 0.36 | 0.08 | 0.56 |
| 2 | $\beta_\theta$ | 0.13 | 0.03 | 0.84 |

TABLE XVII. Probability $p_{SA}$ that the proposed walk is self-avoiding for the reptation move in two and three dimensions. We consider noninteracting SAWs.

| $d$ | $N=100$ | $N=300$ | $N=1000$ |
|---|---|---|---|
| 2 | 0.882 | 0.880 | 0.880 |
| 3 | 0.938 | 0.937 | 0.937 |

It is interesting to compute the probability of a successful move. For noninteracting SAWs such a probability is the product of two terms: the probability $p_{pr}$ that a given move is proposed and the probability $p_{SA}$ that the proposed walk is self-avoiding. At the $\theta$-point one must additionally multiply by the probability that the Metropolis test is successful. Numerical estimates of these probabilities are reported in Tables XIV and XV. Note that they have a very weak $N$ dependence and clearly approach a constant value as $N$ goes to infinity.

Using the above presented results, we can compute the probability of a successful move. They are reported in Table XVI. Note that at the $\theta$ point the probability of a null transition is quite large and in particular B22 moves are quite rarely performed.

### 2. Reptation move

There are two different implementations of the reptation (or slithering-snake) move. The first one, which satisfies detailed balance, works as follows (*Version 1*):

*Step 1*. With probability 1/2 delete $\omega[N-1,N]$ and add a new link at the beginning of the walk; otherwise, delete $\omega[0,1]$ and add a new link at the end of the walk.

*Step 2*. Check if the new walk is self-avoiding. If it is keep it, otherwise perform a null transition.

*Step 3*. Compute the difference in energy between the old and the new walk and perform a Metropolis test.

A second version uses an additional flag that specifies which of $\omega(0)$ and $\omega(N)$ is the ''active'' end point. It works as follows [*Version 2*]:

*Step 1*. Delete one bond at the ''active'' end point and append a new one at the opposite end of the walk.

*Step 2*. If the new walk is self-avoiding keep it, otherwise stay with the old walk, and change the flag, switching the active end point.

*Step 3*. Compute the difference in energy between the old and the new walk and perform a Metropolis test.

This algorithm does not satisfy detailed balance, but it satisfies the stationarity condition generating the correct probability distribution.

It is interesting to compute the probability of success of a reptation move. In the absence of interactions it is simply given by the probability that the proposed walk is self-avoiding. Such a probability is reported in Table XVII. The reptation move is quite successful, being accepted with high probability in both two and three dimensions.

TABLE XVIII. Probability $p_{SA}$ that the proposed walk is self-avoiding and probability $p_{Met}$ that the proposed self-avoiding walk is accepted in the Metropolis test. For reptation moves, we consider SAWs in two dimensions at the $\theta$ point.

| | $N=100$ | $N=800$ | $N=1600$ | $N=3200$ |
|---|---|---|---|---|
| $p_{SA}$ | 0.643 | 0.566 | 0.551 | 0.540 |
| $p_{Met}$ | 0.697 | 0.663 | 0.658 | 0.654 |

At the $\theta$ point, we must also consider the probability that the proposed walk passes the Metropolis test. Numerical results are reported in Table XVIII. Since the walk is more compact, $p_{SA}$ is lower than in the noninteracting case, although still quite large. Multiplying the two probabilities we see that the reptation move is accepted in 35% of the cases. Note that this probability is larger than the probability of a local or bilocal B22 move, see Table XVI.

### 3. Kink-end/end-kink move

The kink-end/end-kink move uses BKE moves (see Fig. 3). It consists of the following steps:

*Step 1*. Choose a random site $i$ of the current walk with $0 \leqslant i \leqslant N-2$.

*Step 2*. Propose an end-kink move with probability $(2d-2)p$ or a kink-end move with probability $(2d-1)^2 p$. In the first case delete the last two bonds of the walk and insert a kink on the bond $\Delta\omega(i)$ in one of the $(2d-2)$ possible orientations. In the second case, if $i \neq 0$ and $\omega[i-1,i+2]$ is a kink, remove it and attach two bonds at the end of the walk in one of the $(2d-1)^2$ possible ways. Otherwise, perform a null transition and the iteration ends.

*Step 3*. Check if the proposed walk is self-avoiding. If it is keep it, otherwise make a null transition.

*Step 4*. Compute the difference in energy between the old and the new walk and perform a Metropolis test.

The fastest dynamics is obtained [16] for $p=1/11$ in $d=2$, and $p=1/29$ in $d=3$. A slightly more efficient implementation is discussed in Ref. [16].

We have computed numerically the probability that a kink-end or an end-kink move is accepted. We find 0.140, 0.138, 0.138 for $N=100,300,700$, respectively. The probability of a null transition is, therefore, quite large, much larger than for a kink-kink bilocal move. Note, however, that a kink-end/end-kink move is performed more often than a B22 move and thus this type of moves should be slightly more efficient in updating the part of the walk that is far from the end points than B22 moves.


[1] P. G. de Gennes, *Scaling Concepts in Polymer Physics* (Cornell University Press, Ithaca, NY, 1979).
[2] J. des Cloizeaux and G. Jannink, *Les Polymères en Solution* (Les Editions de Physique, Les Ulis, 1987); English translation: *Polymers in Solution: Their Modeling and Structure* (Oxford University Press, Oxford, 1990).
[3] K.F. Lau and K.A. Dill, Macromolecules **22**, 3986 (1989).
[4] A. Sali, E. Shakhnovich, and M. Karplus, Nature (London) **369**, 248 (1994).
[5] P.H. Verdier and W.H. Stockmayer, J. Chem. Phys. **36**, 227 (1962).
[6] A.K. Kron, Vysokomol. Soedin. Ser. A **7** 1228 (1965) [Polym. Sci. U.S.S.R. **7**, 1361 (1965)].
[7] A.K. Kron, O.B. Ptitsyn, A.M. Skvortsov, and A.K. Fedorov, Mole. Biol. (Moscow) **1**, 576 (1967) [Mol. Biol. (Moscow) **1**, 487 (1967)].
[8] F.T. Wall and F. Mandel, J. Chem. Phys. **63**, 4592 (1975).
[9] F. Mandel, J. Chem. Phys. **70**, 3984 (1979).
[10] N. Madras and A.D. Sokal, J. Stat. Phys. **47**, 573 (1987).
[11] N. Madras and G. Slade, *The Self-Avoiding Walk* (Birkhäuser, Boston, 1996).
[12] It should be noted that the ergodicity problem is less severe for reptation than for local algorithms. For instance, for reptation one can prove (see Ref. [10] and Proposition 9.2.3 in Ref. [11]) that the fraction of walks belonging to the ergodicity class of the straight rod is larger than $\sim N^{-(\gamma-1)/2}$. On the other hand, for local algorithms, each ergodicity class contains only an exponentially small fraction of the walks.
[13] M. Karplus and E. Shakhnovich, *Protein Folding* (Freeman, New York, 1992).
[14] J.D. Bryngelson, J.N. Onuchic, N.D. Socci, and P.G. Wolynes, Proteins: Struct., Funct., Genet. **21**, 167 (1995).
[15] *Monte Carlo Approach to Biopolymers and Protein Folding*, edited by P. Grassberger, G. T. Barkema, and W. Nadler (World Scientific, Singapore, 1998).
[16] S. Caracciolo, M.S. Causo, G. Ferraro, M. Papinutto, and A. Pelissetto, J. Stat. Phys. **100**, 1111 (2000).
[17] B. Berg and D. Foerster, Phys. Lett. B **106**, 323 (1981).
[18] C. Aragão de Carvalho and S. Caracciolo, J. Phys. (France) **44**, 323 (1983).
[19] C. Aragão de Carvalho, S. Caracciolo, and J. Fröhlich, Nucl. Phys. B **215**, 209 (1983).
[20] A. Berretti and A.D. Sokal, J. Stat. Phys. **40**, 483 (1985).
[21] K. Suzuki, Bull. Chem. Soc. Jpn. **41**, 538 (1968).
[22] S. Redner and P.J. Rednolds, J. Phys. A **14**, 2679 (1981).
[23] P. Grassberger, Phys. Rev. E **56**, 3682 (1997).
[24] P. Grassberger and W. Nadler, e-print cond-mat/0010265.
[25] M. Lal, Mol. Phys. **17**, 57 (1969).
[26] B. MacDonald, N. Jan, D.L. Hunter, and M.O. Steinitz, J. Phys. A **18**, 2627 (1985).
[27] N. Madras and A.D. Sokal, J. Stat. Phys. **50**, 109 (1988).
[28] N. Madras, A. Orlitsky, and L.A. Shepp, J. Stat. Phys. **58**, 159 (1990).
[29] S. Caracciolo, A. Pelissetto, and A.D. Sokal, J. Stat. Phys. **67**, 65 (1992).
[30] T. Kennedy, e-print cond-mat/0109308.
[31] J. Reiter, Macromolecules **23**, 3811 (1990).
[32] O. Jagodzinski, E. Eisenriegler, and K. Kremer, J. Phys. I **2**, 2243 (1992).
[33] J. Skolnick and A. Kolinski, J. Mol. Biol. **221**, 499 (1991).

[34] It should be noted that the algorithm of Ref. [32] is not ergodic.
[35] P. Belohorec and B. G. Nickel (unpublished).
[36] A. Pelissetto and E. Vicari, e-print cond-mat/0012164.
[37] B. Duplantier and H. Saleur, Phys. Rev. Lett. **59**, 539 (1987).
[38] M.J. Stephen, Phys. Lett. **53A**, 363 (1975).
[39] B. Duplantier, J. Phys. (France) **43**, 991 (1982).
[40] B. Duplantier, Europhys. Lett. **1**, 491 (1986).
[41] B. Duplantier, J. Chem. Phys. **86**, 4233 (1987).
[42] P. Grassberger and R. Hegger, J. Phys. I **5**, 597 (1995).
[43] G.T. Barkema, U. Bastolla, and P. Grassberger, J. Stat. Phys. **90**, 1311 (1998).
[44] M.C. Tesi, E.J. Janse van Rensburg, E. Orlandini, and S.G. Whittington, J. Phys. A **29**, 2451 (1996).
[45] A. D. Sokal, in *Monte Carlo and Molecular Dynamics Simulations in Polymer Science*, edited by K. Binder (Oxford University Press, Oxford, 1995).
[46] See Algorithm C, p. 514, and Exercise 23 in Sec. 6.4 of D. E. Knuth, *The Art of Computer Programming* (Addison Wesley, Reading, MA, 1973), Vol. 3.
[47] B. Li, N. Madras, and A.D. Sokal, J. Stat. Phys. **80**, 661 (1995).
[48] P.C. Hohenberg and B.I. Halperin, Rev. Mod. Phys. **49**, 435 (1977).
[49] S. Caracciolo, A. Pelissetto, and A.D. Sokal, J. Stat. Phys. **60**, 1 (1990).
[50] Note that "possible" directions means here a direction for which there are no intersections with $\omega[i-1,i+2]$. It is worth mentioning that an I (respectively, S, L) always has $(2d-2)$ [respectively, $(2d-4)$, $(2d-3)$] possible directions.